Machine Copy for Proofreading, Vol. x, y–z, 2004

ERROR CONTROL OF THE VECTORIAL NONDIRECTIVE STABLE PLANE WAVE MULTILEVEL FAST MULTIPOLE ALGORITHM

Ignace Bogaert, Joris Peeters and Daniël De Zutter ***Fellow IEEE***

Department of Information Technology (INTEC), Ghent University

Sint-Pietersnieuwstraat 41, B-9000 Gent, Belgium

Email:
Ignace.Bogaert@intec.UGent.be,
Joris.Peeters@intec.UGent.be,
Daniel.DeZutter@intec.UGent.be

Abstract—Novel formulas are presented that allow the rapid estimation of the number of terms L that needs to be taken into account in the translation operator of the *vectorial* Nondirective Stable Plane Wave Multilevel Fast Multipole Algorithm (NSPWMLFMA). This is especially important for low frequencies, since the L needed for error-controllability can be substantially higher than the L required in the scalar case. Although these formulas were originally derived for use in the NSPWMLFMA, they are equally useful in at least three other fast matrix multiplication methods.

1. INTRODUCTION

When integral equations for electromagnetic scattering are iteratively solved, the computationally most intensive step is the multiplication of the system matrix with a vector. In essence, this is the calculation of the fields generated by a collection of sources. When there are N sources and N points where the fields need to be calculated (observation points), N^2 operations are needed. In the past, many fast matrix multiplication methods (FMMMs) have been developed to perform this task more efficiently, usually reducing the complexity to $\mathcal{O}(N)$ or $\mathcal{O}(N \log N)$ [1–7]. This reduction of the complexity is achieved by subdividing the geometry of the problem into a hierarchy of boxes (usually called a tree) and invoking a decomposition of the Green function to let the boxes interact as a whole. Figure 1 shows such a possible configuration of boxes.

Because a decomposition of the Green dyadic is used instead of the Green dyadic itself, an error is introduced, making FMMMs inherently approximate. Therefore, it is of the utmost importance that the error

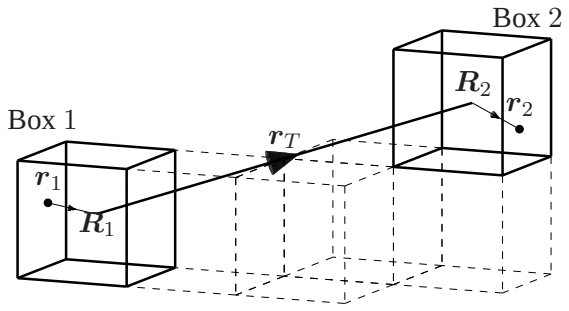

Figure 1. An example box configuration.

introduced by decomposing the Green dyadic is tightly controlled. This error-control takes different forms in different FMMMs. For example, in multipole or Taylor series decompositions, the number of terms in the series is increased to obtain a higher accuracy. In plane wave based FMMMs, the number of radiation pattern samples is increased. However, some FMMMs have certain commonalities. More specifically the Multilevel Fast Multipole Algorithm (MLFMA), its multipole-based equivalent [8], the Nondirective Stable Plane Wave Multilevel Fast Multipole Algorithm (NSPWMLFMA) [9, 10] and the pseudospherical harmonic-based FMMM [11–13] are all based on the following fundamental addition theorem

$$h_0^{(2)}(kr) \approx \sum_{l=0}^{L} (-1)^l \tau_{l,l}(r_A, r_T) I(l, \hat{\boldsymbol{r}}_A, l, \hat{\boldsymbol{r}}_T), \tag{1}$$

with $I(l, \hat{\boldsymbol{r}}_A, l, \hat{\boldsymbol{r}}_T)$ given by (B2) from Appendix B and

$$\tau_{l,l'}(r_A, r_T) = \frac{(2l+1)(2l'+1)}{4\pi} h_l^{(2)}(kr_T)\, j_{l'}(kr_A)\,. \tag{2}$$

Here k is the wavenumber, $\boldsymbol{r}_T = \boldsymbol{R}_2 - \boldsymbol{R}_1$ is the translation vector and $\boldsymbol{r}_A = \boldsymbol{r}_2 - \boldsymbol{r}_1 - \boldsymbol{r}_T$ is called the aggregation vector. Normalized vectors are denoted with a hat, and the norm of a vector is denoted by the same symbol as the vector but non-bold, so for example $\boldsymbol{r}_A = r_A \hat{\boldsymbol{r}}_A$ and $\boldsymbol{r}_T = r_T \hat{\boldsymbol{r}}_T$. Also, $\boldsymbol{r} = \boldsymbol{r}_A + \boldsymbol{r}_T$ is the sum of the aggregation and translation vector and $j_l(\cdot)$ and $h_l^{(2)}(\cdot)$ are the spherical Bessel and Hankel functions. Since these four FMMMs all derive from the same addition theorem, their number of multipoles or sample points can be obtained from the truncation bound of (1), i.e. L. For example in the MLFMA, the number of plane waves is $(L+1)(2L+1)$ while in the NSPWMLFMA the number of plane waves is $(L+1)^2$. In the pseudospherical harmonic-based FMMM, the maximum order of the pseudospherical harmonics is L and finally, in the multipole-based FMMM, the maximum order of the spherical Hankel functions in the translation matrices is L. Therefore, an efficient and simple way to estimate L is very useful for at least four FMMMs. First of all, having an estimate for L is very valuable from a theoretical point of view for understanding of the error behavior of an FMMM. Also, it is useful in a solver if L is calculated on-the-fly. Indeed, in such a solver L is usually determined by means of a numerical testing approach, i.e. the truncation bound is set at an initial estimate, and then gradually adjusted until the error in some testing scenario has been reduced to just below the target accuracy ε. This numerical testing yields quasi-optimal results but can take a long time in the setup phase if the initial estimate for L is not close to the final value. Therefore, if a good initial estimate of the truncation bound can be found quickly, this entire process can be sped up by an order of magnitude. A considerable amount of literature is

devoted to finding dedicated formulas for initial estimates of L in various frequency ranges. For example, the excess bandwidth formula, presented in [14] provides an initial estimate for the high-frequency (HF) case. In [15,16], the excess bandwidth formula is supplemented with additional formulas such that L can be estimated for medium frequencies also. For low frequencies (LF), dedicated formulas can also be derived.

However, these approximate formulas only guarantee the requested relative precision when evaluating the Green function. Clearly, if serious cancelation occurs between two evaluations at slightly different positions, the final result can have a much higher relative error. Unfortunately, this is exactly what happens when evaluating the electric and magnetic Green dyadic arising from Maxwell's equations. Indeed, the spatial derivatives occurring in the electric and magnetic Green dyadic can be interpreted as the limit of $\frac{h_0^{(2)}(kr)-h_0^{(2)}(k||\boldsymbol{r}-\Delta\boldsymbol{d}||)}{\Delta}$ for vanishing Δ. The vector $\boldsymbol{d}$ is the direction in which the derivative is taken. Clearly this process entails serious numerical cancelations.

The aim of this paper is the development of formulas for the estimation of L when evaluating the electric and magnetic Green dyadic. For the HF case, this work has already been accomplished in [8] (see pages 88-92). The conclusion was that the scalar L had to be increased by 1 and 2 for the magnetic and electric Green dyadic respectively. However, to the best knowledge of the authors, no work has to this date been published that treats the L determination in the medium and low frequency ranges for the magnetic and electric Green dyadic. In the following, it will be shown that simply adding 1 or 2 to the scalar L does not lead to a controlled error.

To avoid developing a patchwork of approximate formulas, each of them valid in a specific frequency range, we will not extend the estimation formulas from the literature to the dyadic case but rather start from a slightly modified version of an approach proposed in [9]. This approach works for all frequencies, hence we only need to extend one formula to the dyadic case. In the slightly modified version of the approach in [9], L is chosen such that the relative error on (1), defined by

$$E_s(L,\boldsymbol{r}_A,\boldsymbol{r}_T) = \frac{\left|h_0^{(2)}(kr) - \sum_{l=0}^{L}(-1)^l \tau_{l,l}(r_A,r_T) I(l,\hat{\boldsymbol{r}}_A,l,\hat{\boldsymbol{r}}_T)\right|}{\left|h_0^{(2)}(kr)\right|}, \tag{3}$$

is smaller than the target accuracy ϵ. The values for $\boldsymbol{r}_A$ and $\boldsymbol{r}_T$ must be chosen such that any other choice would result in a smaller error, i.e. they must be the worst case scenario. In practice, it turns out that the error E_s is maximal if $\boldsymbol{r}_A$ and $\boldsymbol{r}_T$ are aligned (and otherwise arbitrarily oriented), because then the Legendre polynomial in (B2) attains the maximal amplitude.

As a consequence, $\boldsymbol{r}_A = r_B\hat{\boldsymbol{e}}_z$ and $\boldsymbol{r}_T = r_T\hat{\boldsymbol{e}}_z$ is usually a very good choice, with r_B the maximal value r_A can attain, i.e. $\sqrt{3}$ times the side of the boxes in Figure 1. Clearly, checking at which value for L the error (3) drops below the target accuracy is an algorithm of $\mathcal{O}(L)$ computational complexity, which is very computationally cheap. The result obtained by means of formula (3) provides an excellent estimate for L that can, if wanted, be refined using a numerical testing scheme.

The layout of this paper is as follows: In Section 2 the electric and magnetic Green dyadics are briefly introduced, along with their plane wave representation as used in the MLFMA. In Section 3, the cancelation that leads to the loss of precision will be more thoroughly demonstrated, taking the electric field integral equation (EFIE) as an example. It will also be shown that it is possible to compensate for the deleterious effects of cancelation by using a higher L than the one obtained from equation (3). In Section 4, formulas similar to (3) are presented for the approximate determination of this new L. Finally, in Section 5 some numerical results will be reported and discussed.

It will be assumed that the reader is familiar with the MLFMA or related techniques. For a detailed discussion of the method we refer to [9] and [8]. Also, a $e^{j\omega t}$ time dependence will be assumed and suppressed throughout this paper.

2. THE VECTORIAL Multilevel Fast Multipole Algorithm

The Green function of the scalar Helmholtz equation is given by

$$G_0(\boldsymbol{r}) = \frac{e^{-jkr}}{4\pi r} = -\frac{jk}{4\pi}h_0^{(2)}(kr), \tag{4}$$

and satisfies

$$\boldsymbol{\nabla}^2 G_0(\boldsymbol{r}) + k^2 G_0(\boldsymbol{r}) = -\delta(\boldsymbol{r}). \tag{5}$$

The electric and magnetic Green dyadics used in this paper are given by

$$\mathsf{G}_e(k\boldsymbol{r}) = \left[\mathbb{1} + \frac{1}{k^2}\boldsymbol{\nabla}\boldsymbol{\nabla}\right] h_0^{(2)}(kr), \tag{6}$$

and

$$\mathsf{G}_m(k\boldsymbol{r}) = \frac{1}{k}\boldsymbol{\nabla} \times \left[\mathbb{1} h_0^{(2)}(kr)\right]. \tag{7}$$

In the above, $\mathbb{1}$ is the 3 by 3 identity matrix.

We now turn to constructing plane wave integral representations for the Green dyadics (6) and (7). For this, the vector $\boldsymbol{r}$ is again seen as the

sum of $\boldsymbol{r}_A$ and $\boldsymbol{r}_T$. The scalar MLFMA is based on the following integral representation of the spherical Hankel function of the second kind

$$h_0^{(2)}(kr) \approx \frac{1}{4\pi}\int_{\mathcal{S}_2} T_L(k\boldsymbol{r}_T, \hat{\boldsymbol{k}}) e^{-jk\hat{\boldsymbol{k}}\cdot\boldsymbol{r}_A} \mathrm{d}\hat{\boldsymbol{k}}, \tag{8}$$

with the so-called translation operator defined by

$$T_L(k\boldsymbol{r}_T, \hat{\boldsymbol{k}}) = \sum_{l=0}^{L} j^{-l}(2l+1) h_l^{(2)}(kr_T)\, P_l\Big(\hat{\boldsymbol{r}}_T \cdot \hat{\boldsymbol{k}}\Big). \tag{9}$$

The integral with subscript $\mathcal{S}_2$ denotes integration over the unit sphere

$$\int_{\mathcal{S}_2} F(\hat{\boldsymbol{k}})\mathrm{d}\hat{\boldsymbol{k}} = \int_0^{2\pi}\int_0^{\pi} F(\hat{\boldsymbol{k}}(\theta,\phi))\sin\theta \mathrm{d}\theta\mathrm{d}\phi, \tag{10}$$

with the wavevector

$$\hat{\boldsymbol{k}}(\theta,\phi) = \begin{bmatrix} \cos\phi\sin\theta \\ \sin\phi\sin\theta \\ \cos\theta \end{bmatrix}. \tag{11}$$

Expression (8) is approximate because of the truncation of the series in (9).

Following [8], substituting the integral representation of the scalar Green function (8) into (28) and (29) yields integral representations of the electric and magnetic Green dyadics

$$\mathsf{G}_e(k\boldsymbol{r}) \approx \frac{1}{4\pi}\int_{\mathcal{S}_2} T_L(k\boldsymbol{r}_T, \hat{\boldsymbol{k}}) \left[\mathbb{1} - \hat{\boldsymbol{k}}\hat{\boldsymbol{k}}\right] e^{-jk\hat{\boldsymbol{k}}\cdot\boldsymbol{r}_A} \mathrm{d}\hat{\boldsymbol{k}}, \tag{12}$$

and

$$\mathsf{G}_m(k\boldsymbol{r}) \approx \frac{j}{4\pi}\int_{\mathcal{S}_2} T_L(k\boldsymbol{r}_T, \hat{\boldsymbol{k}}) \left[\mathbb{1} \times \hat{\boldsymbol{k}}\right] e^{-jk\hat{\boldsymbol{k}}\cdot\boldsymbol{r}_A} \mathrm{d}\hat{\boldsymbol{k}}. \tag{13}$$

These expressions have been used in the literature to construct a fully vectorial MLFMA which uses only two radiation patterns for each MLFMA box [8].

For the HF case, the excess bandwidth formula can be adjusted [8] to give an L that is appropriate for the vectorial case. For the LF case, however, this adjustment is not sufficient.

3. CANCELLATION IN THE EFIE

To demonstrate the occurrence of numerical cancelation, we will consider the calculation of electric field integral equation (EFIE) matrix elements. These

matrix elements are defined as

$$[\mathsf{Z}]_{nm} = \int \boldsymbol{t}_n(\boldsymbol{r}) \cdot \int \mathsf{G}_e(\boldsymbol{r}-\boldsymbol{r}') \cdot \boldsymbol{b}_m(\boldsymbol{r}')\mathrm{d}S'\mathrm{d}S. \tag{14}$$

with $\boldsymbol{t}_n(\boldsymbol{r})$ and $\boldsymbol{b}_m(\boldsymbol{r}')$ the test and basis functions respectively. In this section, we will use the familiar RWGs [17]. Due to the div-conformity of these functions, the EFIE matrix elements can be cast in the mixed-potential form

$$\begin{aligned}[\mathsf{Z}]_{nm} &= \int\int h_0^{(2)}\left(k\,||\boldsymbol{r}-\boldsymbol{r}'||\right)\boldsymbol{t}_n(\boldsymbol{r})\cdot\boldsymbol{b}_m(\boldsymbol{r}')\mathrm{d}S'\mathrm{d}S \\ &+ \frac{1}{k^2}\int\int \left[\boldsymbol{\nabla}\cdot\boldsymbol{t}_n(\boldsymbol{r})\right] h_0^{(2)}\left(k\,||\boldsymbol{r}-\boldsymbol{r}'||\right)\left[\boldsymbol{\nabla}\cdot\boldsymbol{b}_m(\boldsymbol{r}')\right]\mathrm{d}S'\mathrm{d}S. \end{aligned} \tag{15}$$

The surface divergence of the RWGs consists of two adjacent triangular patches on which an equal but opposite charge is uniformly distributed. The proximity of the two patches and the fact that they have an opposite sign causes a cancelation between the contributions from these two patches, leading to a severe deterioration of the accuracy.

As a numerical example, consider the RWGs depicted in Figure 2. The boxes depicted in solid lines have a total of 16 RWGs associated with them, i.e. 2 RWGs on every vertex. For example, on the vertex with location $\frac{1}{2}\left[\hat{\boldsymbol{e}}_x+\hat{\boldsymbol{e}}_y+\hat{\boldsymbol{e}}_z\right]$, the first RWG is defined by the triangles $\Delta\left(\boldsymbol{a}_1,\boldsymbol{a}_2,\boldsymbol{a}_3\right)$ and $\Delta\left(\boldsymbol{a}_2,\boldsymbol{a}_3,\boldsymbol{a}_4\right)$, while the second RWG is defined by the triangles $\Delta\left(\boldsymbol{a}_1,\boldsymbol{a}_2,\boldsymbol{a}_4\right)$ and $\Delta\left(\boldsymbol{a}_1,\boldsymbol{a}_3,\boldsymbol{a}_4\right)$, with

$$\boldsymbol{a}_1 = \frac{\sqrt{3}}{2}\hat{\boldsymbol{k}}(\theta_0+\delta_\theta,\phi_0), \tag{16a}$$

$$\boldsymbol{a}_2 = \frac{\sqrt{3}}{2}\hat{\boldsymbol{k}}(\theta_0,\phi_0+\delta_\phi), \tag{16b}$$

$$\boldsymbol{a}_3 = \frac{\sqrt{3}}{2}\hat{\boldsymbol{k}}(\theta_0,\phi_0-\delta_\phi), \tag{16c}$$

$$\boldsymbol{a}_4 = \frac{\sqrt{3}}{2}\hat{\boldsymbol{k}}(\theta_0-\delta_\theta,\phi_0), \tag{16d}$$

$$\theta_0 = \arccos\left(\frac{1}{\sqrt{3}}\right), \tag{16e}$$

$$\phi_0 = \frac{\pi}{4}, \tag{16f}$$

$$\delta_\theta = \delta_\phi = 0.2 \tag{16g}$$

In this way, the two RWGs are sensitive to two orthogonal field components. In addition, all the RWGs are on the edge of the range where the addition

theorem (1) is supposed to have controllable accuracy, hence they provide a suitable worst case testing scenario.

The RWGs in the lower box will be taken as the basis functions $\boldsymbol{b}_m(\boldsymbol{r}')$ while the RWGs in the upper box will be the test functions $\boldsymbol{t}_n(\boldsymbol{r})$. The EFIE matrix elements are both computed exactly using (6) and using the NSPWMLFMA for the case $k = 0.01\text{m}^{-1}$. To evaluate the worst-case error between the two matrices, we will define an error associated with a so-called vertex pair. Such a pair consists of one of the 8 vertices of the lower box and one of the 8 vertices of the upper box. Obviously, there are in total 64 such vertex pairs. Also, there are two RWGs located at each vertex, which allows us to compute a 2×2 EFIE matrix Z_{n_1,n_2} for each vertex pair (n_1 and n_2 denote the indices of the two vertices in their respective boxes). The error on this EFIE matrix will be defined as

$$D_e^{n_1,n_2} = \frac{\left|\left|\mathsf{Z}^{\text{NSPWMLFMA}}{}_{n_1,n_2} - \mathsf{Z}^{\text{Exact}}{}_{n_1,n_2}\right|\right|}{\left|\left|\mathsf{Z}^{\text{Exact}}{}_{n_1,n_2}\right|\right|}. \tag{17}$$

The worst-case error will now be evaluated as the maximum error over all possible vertex pairs

$$D_e = \max_{n_1,n_2}\left(D_e^{n_1,n_2}\right). \tag{18}$$

Figure 3 shows the actual calculated error on the matrix and the predicted error $E_s(L, \sqrt{3}\hat{\boldsymbol{e}}_z, 3\hat{\boldsymbol{e}}_z)$ for various values of L. Clearly, the actual error decreases much more slowly than the error predicted by (3). The fact that we used the mixed-potential formulation of the EFIE is not the cause of this, since numerical experiments show that the slow convergence still occurs when the dyadic formulation is used. This leads us to conclude that the electric Green dyadic itself converges more slowly to the correct result, and that a suitable L can be found for which the target accuracy is obtained.

In the next Section we will search for a formula of similar simplicity as equation (3) for the determination of L for the electric and magnetic Green dyadic. For some basic mathematical properties of the Legendre polynomials and spherical harmonics, to be used in the sequel, the reader is referred to Appendix A.

4. DETERMINING L FOR THE DYADIC Green functions

Using the orthogonality of the spherical harmonics (A8) and the spherical harmonic addition theorem (A9), the integral representation (8) is easily shown to reduce to (1). Clearly, if L is chosen large enough such that (1) has converged with a tolerance ϵ, then (8) has also converged with the same accuracy. In practice, there are other sources of errors such as numerical

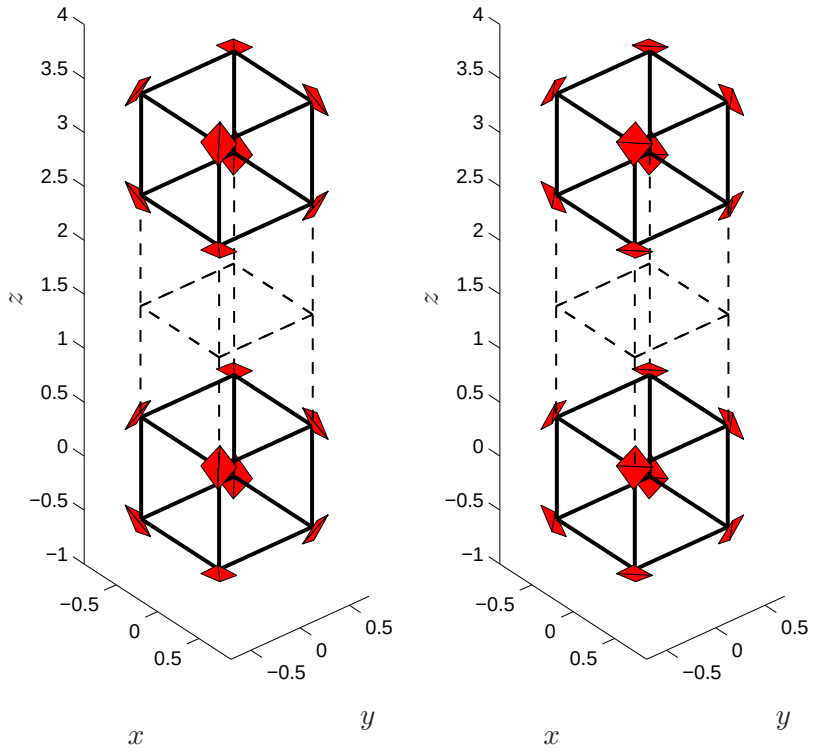

Figure 2. The used RWGs.

interpolation error, integration error, roundoff error, etc. However, these errors can always be assumed to be of the same magnitude as ϵ. Indeed, if one source of error would greatly dominate, it would be advantageous to make the other sources of error larger as well, since doing so reduces the computational burden. Therefore we will assume that these other error generating mechanisms are not dominant. Under this assumption, it is clear that (3) yields a reasonably good approximation for L in the scalar case.

In the vectorial case the following question naturally arises: can the integral representations (12) and (13) be reduced to an expression as simple as (1) ? In the following, this question will be answered in the affirmative.

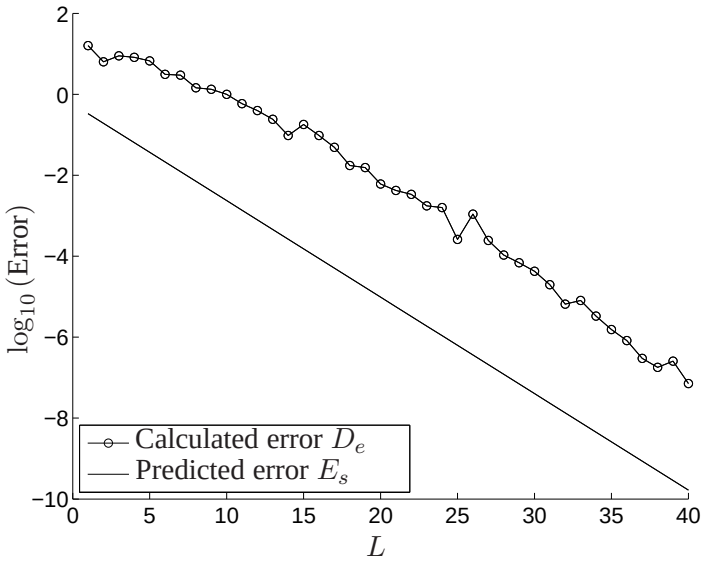

Figure 3. The calculated error on the electric Green dyadic, given in Eqn. (18), does not converge as predicted by formula (3).

4.1. The magnetic Green dyadic

Equation (13) is a plane wave decomposition of the magnetic Green dyadic. Using the well-known Jacobi-Anger expansion of a plane wave

$$e^{-jk\hat{\boldsymbol{k}}\cdot\boldsymbol{r}_A} = \sum_{l=0}^{\infty}(2l+1)j^{-l}j_l\left(kr_A\right)P_l\Big(\hat{\boldsymbol{k}}\cdot\hat{\boldsymbol{r}}_A\Big)\,, \tag{19}$$

and the explicit expression of the translation operator (9), the following result is easily obtained

$$\mathsf{G}_m(k\boldsymbol{r}) \approx \mathbb{1} \times \sum_{l=0}^{L}(-1)^l\boldsymbol{G}_m^l, \tag{20}$$

with $\boldsymbol{G}_m^l$ given by

$$\begin{aligned}\boldsymbol{G}_m^l = (2l+1)h_l^{(2)}\left(kr_T\right)\sum_{l'=0}^{\infty}\frac{j^{l-l'+1}}{4\pi}(2l'+1)\\ \times j_{l'}\left(kr_A\right)\int_{\mathcal{S}_2}P_l\Big(\hat{\boldsymbol{r}}_T\cdot\hat{\boldsymbol{k}}\Big)\,\hat{\boldsymbol{k}}P_{l'}\Big(\hat{\boldsymbol{k}}\cdot\hat{\boldsymbol{r}}_A\Big)\,\mathrm{d}\hat{\boldsymbol{k}}.\end{aligned} \tag{21}$$

In appendix B, the remaining integral has been evaluated analytically. The result is given by (B3) and allows the elimination of the sum in (21)

$$\begin{aligned}\boldsymbol{G}_m^l = &\tau_{l,l+1}(r_A, r_T)\boldsymbol{I}_{\hat{\boldsymbol{k}}}(l+1, \hat{\boldsymbol{r}}_A, l, \hat{\boldsymbol{r}}_T) \\ &- \tau_{l,l-1}(r_A, r_T)\boldsymbol{I}_{\hat{\boldsymbol{k}}}(l-1, \hat{\boldsymbol{r}}_A, l, \hat{\boldsymbol{r}}_T).\end{aligned} \tag{22}$$

4.2. The electric Green dyadic

For the plane wave representation of the electric Green dyadic, given in (12), we can again use expansion (19) to evaluate the integral as a series

$$\mathsf{G}_e(k\boldsymbol{r}) \approx \sum_{l=0}^{L}(-1)^l \mathsf{G}_e^l, \tag{23}$$

with

$$\begin{aligned}\mathsf{G}_e^l = &\sum_{l'=0}^{\infty} j^{-l'+l}\tau_{l,l'}(r_A, r_T) \\ &\times \int_{\mathcal{S}_2} P_l\left(\hat{\boldsymbol{r}}_T \cdot \hat{\boldsymbol{k}}\right)\left[\mathbb{1} - \hat{\boldsymbol{k}}\hat{\boldsymbol{k}}\right] P_{l'}\left(\hat{\boldsymbol{k}} \cdot \hat{\boldsymbol{r}}_A\right) \mathrm{d}\hat{\boldsymbol{k}}.\end{aligned} \tag{24}$$

The remaining integral can again be evaluated analytically, albeit through significantly more effort. The result is given in appendix B ((B2) and (B10)) and again allows to reduce the infinite sum in (23) to a finite one

$$\begin{aligned}\mathsf{G}_e^l = &\tau_{l,l+2}(r_A, r_T)\mathsf{I}_{\hat{\boldsymbol{k}}\hat{\boldsymbol{k}}}(l+2, \hat{\boldsymbol{r}}_A, l, \hat{\boldsymbol{r}}_T) \\ &+ \tau_{l,l}(r_A, r_T)\left[I(l, \hat{\boldsymbol{r}}_A, l, \hat{\boldsymbol{r}}_T)\mathbb{1} - \mathsf{I}_{\hat{\boldsymbol{k}}\hat{\boldsymbol{k}}}(l, \hat{\boldsymbol{r}}_A, l, \hat{\boldsymbol{r}}_T)\right] \\ &+ \tau_{l,l-2}(r_A, r_T)\mathsf{I}_{\hat{\boldsymbol{k}}\hat{\boldsymbol{k}}}(l-2, \hat{\boldsymbol{r}}_A, l, \hat{\boldsymbol{r}}_T).\end{aligned} \tag{25}$$

4.3. Convergence Criteria

Checking whether series (20) or (23) have converged to the prescribed precision requires a way of comparing the right and left hand side. The problem is that we are dealing with dyadics, and it is not immediately clear which component to choose for calculating the error. Indeed, some components may become exactly zero, such that the relative error of one component is meaningless. To avoid this problem we will use the matrix 2-norm, i.e. the largest singular value, to test the convergence. For more information about the definition of the matrix norm, see [18] from page 54

onwards. Now define the following measures of error

$$E_m(L, \boldsymbol{r}_A, \boldsymbol{r}_T) = \frac{\left|\left|\mathsf{G}_m(k\boldsymbol{r}) - \mathbb{1} \times \sum_{l=0}^{L} (-1)^l \boldsymbol{G}_m^l\right|\right|}{||\mathsf{G}_m(k\boldsymbol{r})||}, \tag{26}$$

$$E_e(L, \boldsymbol{r}_A, \boldsymbol{r}_T) = \frac{\left|\left|\mathsf{G}_e(k\boldsymbol{r}) - \sum_{l=0}^{L} (-1)^l \mathsf{G}_e^l\right|\right|}{||\mathsf{G}_e(k\boldsymbol{r})||}. \tag{27}$$

The matrix norms occurring in these expressions can be computed using SVDs of the 3 by 3 matrices. Surprisingly enough, however, it is possible to find simple and explicit formulas for the matrix norms in the denominators. Indeed, the derivatives occurring in (6) and (7) can be evaluated using (4) and the recurrences for the spherical Hankel functions. For the electric Green dyadic this yields [8]

$$\begin{aligned}\mathsf{G}_e(k\boldsymbol{r}) = h_0^{(2)}(kr) \Bigg[&\left(\frac{2j}{kr} + \frac{2}{(kr)^2}\right) \hat{\boldsymbol{r}}\hat{\boldsymbol{r}} \\ &+ \left(1 - \frac{j}{kr} - \frac{1}{(kr)^2}\right) (\mathbb{1} - \hat{\boldsymbol{r}}\hat{\boldsymbol{r}}) \Bigg],\end{aligned} \tag{28}$$

while the magnetic Green dyadic becomes

$$\mathsf{G}_m(k\boldsymbol{r}) = h_0^{(2)}(kr) \left[\hat{\boldsymbol{e}}_\phi \hat{\boldsymbol{e}}_\theta - \hat{\boldsymbol{e}}_\theta \hat{\boldsymbol{e}}_\phi\right] \left(\frac{1}{kr} + j\right), \tag{29}$$

with $\hat{\boldsymbol{r}}$, $\hat{\boldsymbol{e}}_\phi$ and $\hat{\boldsymbol{e}}_\theta$ the unit vectors in spherical coordinates. The (unsorted) singular values of the Green dyadics are easily found from these formulas, since the singular values of a matrix A are nothing else than the square roots of the eigenvalues of $\mathsf{A}^H\mathsf{A}$. By means of (28) we get the singular values of the electric Green dyadic

$$\sigma_1^e(k\boldsymbol{r}) = \sigma_2^e(k\boldsymbol{r}) = \left| h_0^{(2)}(kr) \left(1 - \frac{j}{kr} - \frac{1}{(kr)^2}\right)\right|, \tag{30}$$

$$\sigma_3^e(k\boldsymbol{r}) = \left| h_0^{(2)}(kr) \left(\frac{2j}{kr} + \frac{2}{(kr)^2}\right)\right|, \tag{31}$$

while for the magnetic Green dyadic, the following singular values are obtained

$$\sigma_1^m(k\boldsymbol{r}) = \sigma_2^m(k\boldsymbol{r}) = \left| h_0^{(2)}(kr) \left(\frac{1}{kr} + j\right)\right|, \tag{32}$$

$$\sigma_3^m(k\boldsymbol{r}) = 0. \tag{33}$$

From this, the denominators in (26) and (27) are found to be

$$||\mathsf{G}_m(k\boldsymbol{r})|| = \sigma_1^m(k\boldsymbol{r}), \tag{34}$$

$$||\mathsf{G}_e(k\boldsymbol{r})|| = \max\left(\sigma_1^e(k\boldsymbol{r}), \sigma_2^e(k\boldsymbol{r})\right). \tag{35}$$

The matrix norm in the numerator of (26) can also be found without using SVDs. Indeed, the matrix norm of an expression of the form $\mathbb{1} \times \boldsymbol{v}$, with $\boldsymbol{v}$ a vector, is simply the vector norm of $\boldsymbol{v}$. Clearly this allows E_m to be calculated more easily as

$$E_m(L, \boldsymbol{r}_A, \boldsymbol{r}_T) = \frac{\left|\left|\hat{\boldsymbol{r}} h_0^{(2)}(kr)\left(\frac{1}{kr} + j\right) - \sum_{l=0}^{L}(-1)^l \boldsymbol{G}_m^l\right|\right|}{\sigma_1^m(k\boldsymbol{r})}. \tag{36}$$

The matrix norm in the numerator of (27) should be computed using the SVD of the 3 by 3 dyadics, as no analytical simplification was found by the authors. However, if one allows an error of a factor $\sqrt{3}$, the Frobenius norm $||\cdot||_F$ (see [18] on page 55) may be used, since it is an equivalent norm for 3 by 3 matrices with bounds

$$\frac{1}{\sqrt{3}}||\mathsf{A}||_F \leq ||\mathsf{A}|| \leq ||\mathsf{A}||_F. \tag{37}$$

5. NUMERICAL RESULTS

As a first test, the L obtained using formulas (3), (26) and (27) are compared to the excess bandwidth formula and the formula presented in [16]. Figure 4 shows the required L as a function of the wavenumber. The parameters for the L calculation are $\boldsymbol{r}_A = \sqrt{3}\hat{\boldsymbol{e}}_z$, $\boldsymbol{r}_T = 3\hat{\boldsymbol{e}}_z$ and the target accuracy is $\varepsilon = 10^{-5}$. It can be seen that, for low frequencies, formula (3), the excess bandwidth formula and the approach from [16] give different results. The difference with the excess bandwidth formula is caused by the fact that the excess bandwidth formula is essentially a high frequency asymptotic approximation for L. The difference with the approach in [16] is caused by the fact that it is focused on the MLFMA. Therefore it has to deal with the MLFMA's inherent numerical instability (low frequency breakdown), which influences the obtained L. For high frequencies, all the L curves approximately go to the same asymptotic limit, i.e. the excess bandwidth formula.

The convergence formulas (26) and (27) will now be numerically tested using the benchmark box configurations shown in Figure 5. The boxes have sides of $1m$. The box configuration on the left depicts the worst-case interaction when two buffer boxes are used, whereas the configuration on the right is the worst-case interaction when only one buffer box is used. Both situations will be studied here.

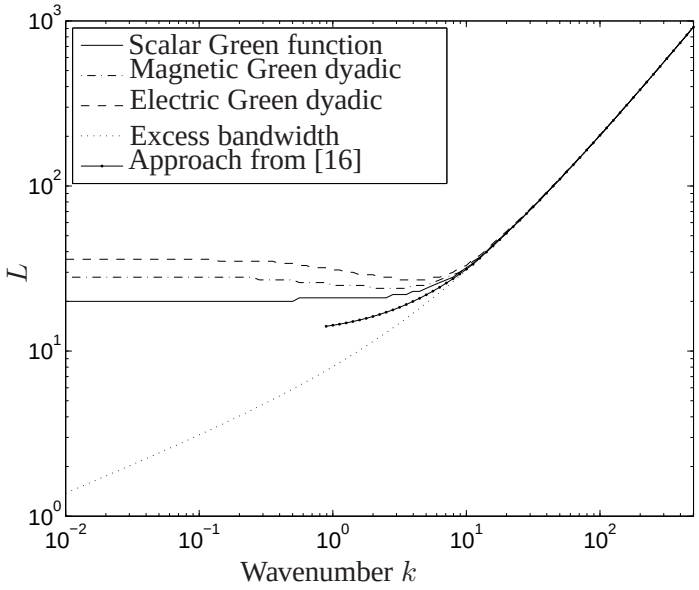

Figure 4. The required L as a function of the wavenumber. The line for the approach from [16] is only shown for wavenumbers for which the MLFMA does not suffer from the low-frequency breakdown (according to [16]).

To compute the error, three elementary dipole sources and observers were put on the vertices of the source and observer boxes in Figure (5). The electric and magnetic fields generated by the source dipoles on the observer dipoles were computed both directly and by means of the NSPWMLFMA (as a function of L). Since these interactions are nothing else than the components of the electric and magnetic Green dyadic, it is possible to compute the following error measures:

$$F_m(L,n_1,n_2) = \frac{\left|\left|\mathsf{G}_m(n_1,n_2) - \mathsf{G}_m^{\text{NSPWMLFMA}}(n_1,n_2)\right|\right|}{||\mathsf{G}_m(n_1,n_2)||}, \tag{38}$$

$$F_e(L,n_1,n_2) = \frac{\left|\left|\mathsf{G}_e(n_1,n_2) - \mathsf{G}_e^{\text{NSPWMLFMA}}(n_1,n_2)\right|\right|}{||\mathsf{G}_e(n_1,n_2)||}, \tag{39}$$

where n_1 and n_2 are the indices of the vertices in the source and observer box. To get the worst-case error, the maximum error is taken

$$F_m(L) = \text{max}_{n_1,n_2}\left[F_m(L,n_1,n_2)\right], \tag{40}$$

$$F_e(L) = \text{max}_{n_1,n_2}\left[F_e(L,n_1,n_2)\right]. \tag{41}$$

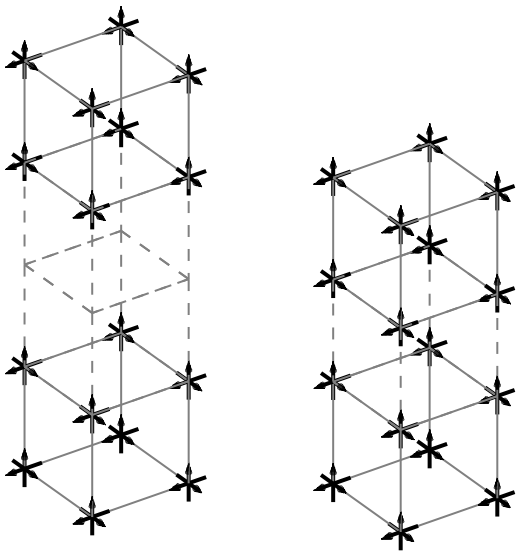

Figure 5. The used benchmark box configurations. The arrows on the vertices of the lower and upper boxes are the dipoles sources and observers respectively.

A similar error measure for the scalar case is also introduced

$$F_s(L) = \max_{n_1,n_2} \left| \frac{G_0(n_1,n_2) - G_0^{\text{NSPWMLFMA}}(n_1,n_2)}{G_0(n_1,n_2)} \right|. \qquad (42)$$

In Figure 6 the calculated error is shown for the two buffer box case. The predicted error $E_e(L, \sqrt{3}\hat{\boldsymbol{e}}_z, 3\hat{\boldsymbol{e}}_z)$ is also plotted. The value $k = 0.01\text{m}^{-1}$ was used for the wavenumber. It is clear that formulas (26) and (27) much better capture the convergence behavior of the magnetic and electric Green dyadic than formula (3). This better approximation of the true behavior also translates into better estimates for L. For example, if one wants an accuracy of 10^{-4}, then (3) would imply $L \approx 16$, while (27) implies $L \approx 31$. From Figure 6, it is seen that $L \approx 30$ would be chosen if L were determined numerically, which is very close to the result obtained using (27).

In Figure 7, the same analysis is performed, with the sole difference being the number of buffer boxes used in the NSPWMLFMA. As can be seen, convergence is very slow. In fact, the result first *diverges* before slowly starting to converge. The slow convergence is not due to the NSPWMLFMA, since formulas (26) and (27) also predict this behavior. It can also be seen that the scalar Green function converges slowly, but steadily. The slow

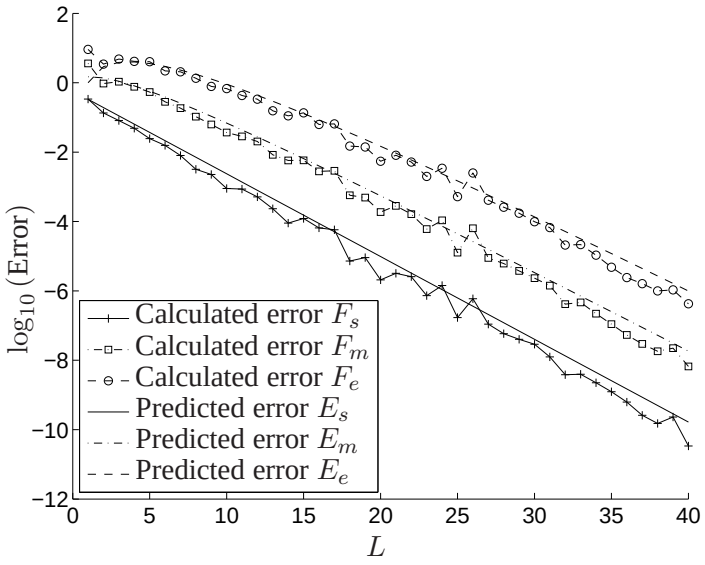

Figure 6. Convergence as a function of the truncation bound L for the scalar Green function, magnetic Green dyadic and the electric Green dyadic for the case where two buffer boxes are used.

convergence of the scalar Green function can be traced back to the fact that the spheres circumscribing the source and observer box almost touch. A quick analysis shows that applying derivatives to the scalar Green function to obtain the electric or magnetic Green dyadic adds factors proportional to L (for the magnetic Green dyadic) or L^2 (for the electric Green dyadic) to the error. These factors are the cause of the diverging error behavior for small L. For large L, the exponential convergence as a function of L is regained, but by then L is impractically large. Therefore, we can conclude that using an FMMM based on spherical modes for the vectorial (dyadic) case at low frequencies and using only one buffer box leads to a huge truncation bound L or, alternatively, to inaccurate results.

The behavior of the error as a function of the wavenumber has also been investigated. Figure 8 shows the calculated and predicted errors for the electric Green dyadic, magnetic Green dyadic and scalar Green function for $L = 20$, using the dipole arrangement with two buffer boxes from Figure 5. As can be seen in Figure 8, the predicted and calculated errors have a very similar behavior which further validates (27) and (26). An interesting phenomenon is the 'dip' that occurs around $k = 4\text{m}^{-1}$ in the error curves for E_e, F_e, E_m and F_m. It appears that, for low frequencies, the truncation bound L *decreases* with increasing frequency. The same effect can also be

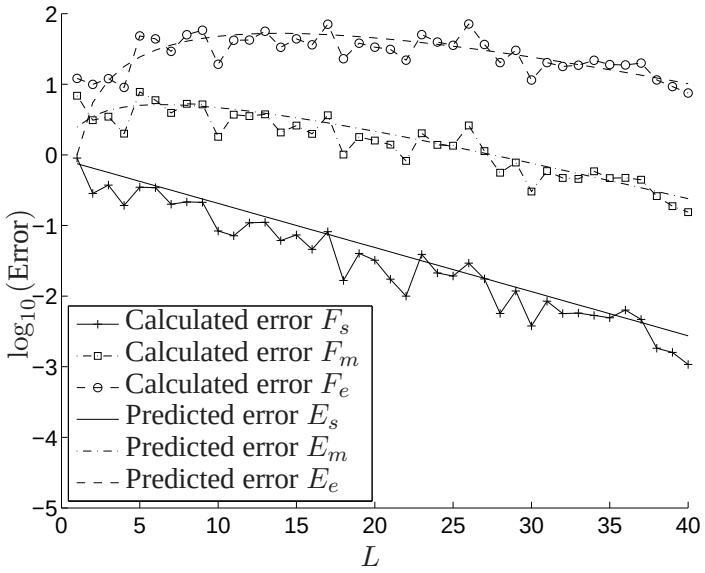

Figure 7. Convergence as a function of the truncation bound L for the scalar Green function, magnetic Green dyadic and the electric Green dyadic for the case where only one buffer box is used.

observed in Figure 4, where the required L for the magnetic and electric Green dyadic exhibits a dip around $k = 4\text{m}^{-1}$. Up to this point, the authors have found no physical or intuitive explanation for this phenomenon.

6. CONCLUSION

Novel formulas were presented that allow the rapid estimation of the number of terms in the translation operator of the vectorial NSPWMLFMA. In contrast to existing estimates for the scalar case, these formulas are tailored to the Green dyadic that is used (electric or magnetic). Some interesting results were obtained. For example, it is shown that the truncation bound obtained from the scalar case is too low when used for the vectorial case at low frequencies. Also at low frequencies, it turns out that the electric Green dyadic requires a higher truncation bound than the magnetic Green dyadic. Hence, when the NSPWMLFMA is used on the EFIE or MFIE at low frequencies, these novel estimates yield a much better error control than estimates for the scalar case. Also, these novel estimates are valuable from a theoretical point of view for understanding of the error behavior of the NSPWMLFMA. In addition, the use of these estimates is not limited to

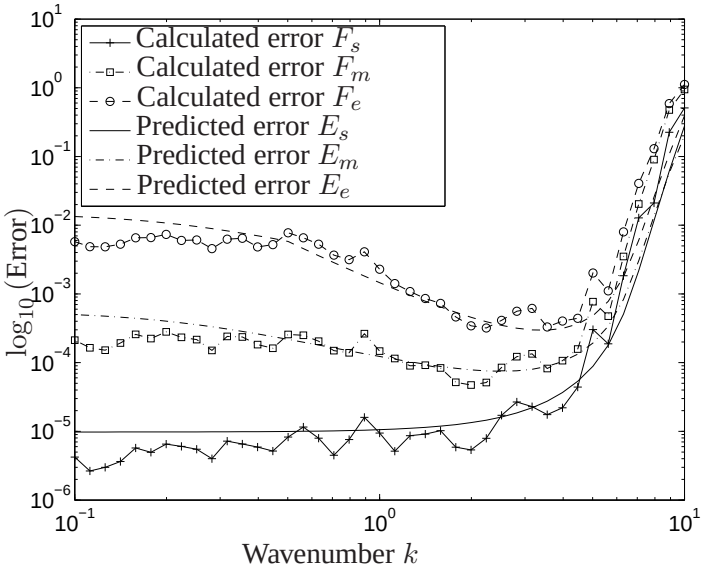

Figure 8. The predicted and calculated error for $L = 20$ as a function of the frequency for the scalar Green function, magnetic Green dyadic and the electric Green dyadic.

the NSPWMLFMA, since they are useful in at least three other fast matrix multiplication methods.

APPENDIX A. SPHERICAL HARMONICS

The Legendre polynomials $P_l(t)$ are defined as

$$P_l(t) = \frac{1}{2^l l!}\frac{\mathrm{d}^l}{\mathrm{d}t^l}(t^2-1)^l, \tag{A1}$$

and satisfy the following recurrence relations

$$(2l+1)tP_l(t) = (l+1)P_{l+1}(t) + lP_{l-1}(t)\,, \tag{A2}$$

$$\begin{aligned}(2l+1)P_l(t) &= \frac{\mathrm{d}}{\mathrm{d}t}\left[P_{l+1}(t) - P_{l-1}(t)\right], \\ &= P'_{l+1}(t) - P'_{l-1}(t)\,.\end{aligned} \tag{A3}$$

The derivative of the Legendre polynomial is denoted as

$$P'_l(t) = \frac{\mathrm{d}}{\mathrm{d}t}P_l(t)\,. \tag{A4}$$

For the stable numerical calculation of the Legendre polynomials, recurrence (A2) should be used with starting values $P_0(t) = 1$ and $P_1(t) = t$.

The spherical harmonics $Y_{l,m}\left(\hat{\boldsymbol{k}}\right)$ are defined as

$$Y_{l,m}\left(\hat{\boldsymbol{k}}\right) = (-1)^{l+m}\frac{K_{l,m}}{2^l l!}\left(\hat{k}_x + j\hat{k}_y\right)^m \mathcal{T}_l^m\left(\hat{k}_z\right). \tag{A5}$$

Here, l and m are integers such that $l \in [0, \infty]$ and $m \in [-l, l]$. Furthermore

$$K_{l,m} = \sqrt{\frac{2l+1}{4\pi}\frac{(l-m)!}{(l+m)!}}, \tag{A6}$$

and

$$\mathcal{T}_l^m(t) = \frac{\mathrm{d}^{l+m}}{\mathrm{d}t^{l+m}}\left[1 - t^2\right]^l, \tag{A7}$$

The spherical harmonics satisfy the following orthogonality relation

$$\int_{\mathcal{S}_2} Y_{l_1,m_1}\left(\hat{\boldsymbol{k}}\right) Y^*_{l_2,m_2}\left(\hat{\boldsymbol{k}}\right) \mathrm{d}\hat{\boldsymbol{k}} = \delta_{l_1,l_2}\delta_{m_1,m_2}. \tag{A8}$$

The spherical harmonics also satisfy the so-called spherical harmonic addition theorem

$$P_l\left(\hat{\boldsymbol{k}}_1 \cdot \hat{\boldsymbol{k}}_2\right) = \frac{4\pi}{2l+1}\sum_{m=-l}^{l} Y^*_{l,m}\left(\hat{\boldsymbol{k}}_1\right) Y_{l,m}\left(\hat{\boldsymbol{k}}_2\right). \tag{A9}$$

APPENDIX B. USEFUL INTEGRALS

In this Appendix, the necessary integrals for this paper are given. For brevity, the dot products $\hat{\boldsymbol{r}}_A \cdot \hat{\boldsymbol{r}}_T$, $\hat{\boldsymbol{r}}_A \cdot \hat{\boldsymbol{k}}$ and $\hat{\boldsymbol{r}}_T \cdot \hat{\boldsymbol{k}}$ will be denoted as γ, γ_A and γ_T respectively. The first integral is

$$I(l_A, \hat{\boldsymbol{r}}_A, l_T, \hat{\boldsymbol{r}}_T) = \int_{\mathcal{S}_2} P_{l_T}(\gamma_T)\, P_{l_A}(\gamma_A)\, \mathrm{d}\hat{\boldsymbol{k}}. \tag{B1}$$

By means of the spherical harmonic addition theorem (A9) and the orthogonality (A8) of the spherical harmonics, the following result is easily obtained

$$I(l_A, \hat{\boldsymbol{r}}_A, l_T, \hat{\boldsymbol{r}}_T) = \delta_{l_A,l_T}\frac{4\pi}{2l_A+1}P_{l_A}(\gamma). \tag{B2}$$

Remember that $\gamma = \hat{\boldsymbol{r}}_A \cdot \hat{\boldsymbol{r}}_T$. The second integral of interest is

$$\boldsymbol{I}_{\hat{\boldsymbol{k}}}(l_A, \hat{\boldsymbol{r}}_A, l_T, \hat{\boldsymbol{r}}_T) = \int_{\mathcal{S}_2} P_{l_T}(\gamma_T)\, \hat{\boldsymbol{k}} P_{l_A}(\gamma_A)\, \mathrm{d}\hat{\boldsymbol{k}}. \tag{B3}$$

This integral could be readily evaluated using the spherical harmonic addition theorem and the recurrences of the spherical harmonics. However the result still contains a sum of $2l+1$ terms, with each term containing a complicated square root. Instead we will derive a closed form for $\boldsymbol{I}_{\hat{\boldsymbol{k}}}$. As a starting point, the following can be shown by means of (A3)

$$\begin{aligned}[\mathbb{1} - \hat{\boldsymbol{r}}_A \hat{\boldsymbol{r}}_A] \cdot \hat{\boldsymbol{k}} P_{l_A}(\gamma_A) \\ = \frac{1}{2l_A+1} \boldsymbol{\nabla}_A \left[P_{l_A+1}(\gamma_A) - P_{l_A-1}(\gamma_A)\right],\end{aligned} \tag{B4}$$

where $\boldsymbol{\nabla}_A = \left[\frac{\mathrm{d}}{\mathrm{d}x_A}, \frac{\mathrm{d}}{\mathrm{d}y_A}, \frac{\mathrm{d}}{\mathrm{d}z_A}\right]$. Since the dot product of $\hat{\boldsymbol{r}}_A$ and $\hat{\boldsymbol{k}}$ in the left hand side can be absorbed into the Legendre polynomial by means of (A2), the following is found

$$\begin{aligned}(2l_A+1)\hat{\boldsymbol{k}} P_{l_A}(\gamma_A) = \\ \boldsymbol{\nabla}_A \left[P_{l_A+1}(\gamma_A) - P_{l_A-1}(\gamma_A)\right] \\ + \hat{\boldsymbol{r}}_A \left[(l_A+1) P_{l_A+1}(\gamma_A) + l_A P_{l_A-1}(\gamma_A)\right].\end{aligned} \tag{B5}$$

This result, combined with (B2), allows us to construct the following closed form expression for $\boldsymbol{I}_{\hat{\boldsymbol{k}}}$

$$\begin{aligned}\boldsymbol{I}_{\hat{\boldsymbol{k}}}(l_A, \hat{\boldsymbol{r}}_A, l_T, \hat{\boldsymbol{r}}_T) = \frac{4\pi}{(2l_T+1)(2l_A+1)} \\ \times \Big\{ \left[(l_A+1)\delta_{l_A+1,l_T} + l_A \delta_{l_A-1,l_T}\right] \hat{\boldsymbol{r}}_A P_{l_T}(\gamma) \\ + \left[\delta_{l_A+1,l_T} - \delta_{l_A-1,l_T}\right] \boldsymbol{\nabla}_A P_{l_T}(\gamma) \Big\}.\end{aligned} \tag{B6}$$

This expression is not very symmetrical but can be simplified using

$$\boldsymbol{\nabla}_A P_{l_T}(\gamma) = \left[\hat{\boldsymbol{r}}_T - \gamma \hat{\boldsymbol{r}}_A\right] P'_{l_T}(\gamma) \tag{B7}$$

and the various recurrences of the Legendre polynomials. The result then becomes

$$\begin{aligned}\boldsymbol{I}_{\hat{\boldsymbol{k}}}(l_A, \hat{\boldsymbol{r}}_A, l_T, \hat{\boldsymbol{r}}_T) = \\ \times 4\pi \frac{\hat{\boldsymbol{r}}_T P'_{l_T}(\gamma) - \hat{\boldsymbol{r}}_A P'_{l_A}(\gamma)}{(2l_A+1)(2l_T+1)} \left[\delta_{l_A+1,l_T} - \delta_{l_A,l_T+1}\right].\end{aligned} \tag{B8}$$

The third and final integral is

$$\mathsf{I}_{\hat{\boldsymbol{k}}\hat{\boldsymbol{k}}}(l_A, \hat{\boldsymbol{r}}_A, l_T, \hat{\boldsymbol{r}}_T) = \int_{\mathcal{S}_2} P_{l_T}(\gamma_T)\, \hat{\boldsymbol{k}}\hat{\boldsymbol{k}} P_{l_A}(\gamma_A)\, \mathrm{d}\hat{\boldsymbol{k}} \tag{B9}$$

The rightmost $\hat{\boldsymbol{k}}$ can again be removed by means of expression (B5). The remaining integral is expressible in terms of $\boldsymbol{I}_{\hat{\boldsymbol{k}}}(l_A, \hat{\boldsymbol{r}}_A, l_T, \hat{\boldsymbol{r}}_T)$ and derivatives thereof. After a lengthy calculation and various simplifications, the following symmetrical form is obtained

$$\begin{aligned}
\mathsf{I}_{\hat{\boldsymbol{k}}\hat{\boldsymbol{k}}}(l_A, \hat{\boldsymbol{r}}_A, l_T, \hat{\boldsymbol{r}}_T) = {} & \frac{4\pi}{(l_A+l_T-1)(l_A+l_T+1)(l_A+l_T+3)} \\
& \times \Big\{ \Big[\hat{\boldsymbol{r}}_T\hat{\boldsymbol{r}}_T P''_{l_T}(\gamma) + \hat{\boldsymbol{r}}_A\hat{\boldsymbol{r}}_A P''_{l_A}(\gamma)\Big] \\
& \qquad \times [\delta_{l_A,l_T+2} - 2\delta_{l_A,l_T} + \delta_{l_A+2,l_T}] \\
& \quad + [\hat{\boldsymbol{r}}_T\hat{\boldsymbol{r}}_A + \hat{\boldsymbol{r}}_A\hat{\boldsymbol{r}}_T] \\
& \qquad \times \Big[\delta_{l_A,l_T}\Big(2\gamma P''_{l_T}(\gamma) + P'_{l_T}(\gamma)\Big) \\
& \qquad\quad - \delta_{l_A,l_T+2} P''_{l_T+1}(\gamma) - \delta_{l_A+2,l_T} P''_{l_A+1}(\gamma)\Big] \\
& \quad + \mathbb{1}\Big[\delta_{l_A,l_T}\Big(2\gamma P'_{l_A}(\gamma) - P_{l_A}(\gamma)\Big) \\
& \qquad\quad - \delta_{l_A,l_T+2} P'_{l_T+1}(\gamma) - \delta_{l_A+2,l_T} P'_{l_A+1}(\gamma)\Big]\Big\}
\end{aligned} \tag{B10}$$

In (B2), (B8) and (B10), the first and second derivatives of the Legendre polynomials need to be evaluated. Calculating these could in principle be done by means of the following recurrence

$$(1-t^2)P'_l(t) = -l(tP_l(t) - P_{l-1}(t)). \tag{B11}$$

However, this calculation is not numerically stable when the argument t is close to ± 1. For a fully stable and robust calculation of $P'_l(t)$ and $P''_l(t)$ for $l \in [0, L]$, all the Legendre polynomials $P_l(t)$ for $l \in [0, L-1]$ should be calculated first. Then recurrence (A3) can be used to determine the first derivatives. For the second derivatives,

$$(2l+1)P'_l(t) = P''_{l+1}(t) - P''_{l-1}(t)\,, \tag{B12}$$

can be used. It is worthwhile to point out that using these techniques, both the Legendre polynomials and their first and second derivatives can be calculated in $\mathcal{O}(L)$ operations. An obvious consequence is that calculating I, $\boldsymbol{I}_{\hat{\boldsymbol{k}}}$ and $\mathsf{I}_{\hat{\boldsymbol{k}}\hat{\boldsymbol{k}}}$ for $l_A \leq L$ and $l_T \leq L$ takes only $\mathcal{O}(L)$ operations.

ACKNOWLEDGMENT

The work of I. Bogaert was supported by a postdoctoral grant from the Fund for Scientific Research (Fonds Wetenschappelijk Onderzoek). The work of J. Peeters was supported by a doctoral grant from the Special Research Fund at Ghent University.

REFERENCES

1. L. Greengard and V. Rokhlin, "A fast algorithm for particle simulations," *Journal of Computational Physics*, vol. 73, no. 2, pp. 325–348, Dec. 1987.
2. R. Coifman, V. Rokhlin, and S. Wandzura, "The fast multipole method for the wave equation: A pedestrian prescription," *IEEE Antennas and Propagation Magazine*, vol. 35, no. 3, pp. 7–12, June 1993.
3. W.C. Chew, J.M. Jin, C.C. Lu, E. Michielssen, and J.M. Song, "Fast solution methods in electromagnetics," *IEEE Transactions on Antennas and Propagation*, vol. 45, no. 3, pp. 533–543, Mar. 1997.
4. J.M. Song, C.C. Lu, W.C. Chew, and S.W. Lee, "Fast Illinois solver code (FISC)," *IEEE Antennas and Propagation Magazine*, vol. 40, no. 3, pp. 27–34, June 1998.
5. E. Darve and P. Havé, "Efficient fast multipole method for low-frequency scattering," *Journal of Computational Physics*, vol. 197, no. 1, pp. 341–363, June 2004.
6. J. Fostier, J. Peeters, I. Bogaert, and F. Olyslager, "An open-source, kernel-independent, asynchronous, parallel MLFMA framework," in *Proceedings of the USNC/URSI National Radio Science Meeting*, San Diego, USA, 5-12 July 2008.
7. J. M. Taboada, M. G. Araujo, J. M. Bertolo, L. Landesa, F. Obelleiro, and J. L. Rodriguez, "Mlfma-fft parallel algorithm for the solution of large-scale problems in electromagnetics," *Progress In Electromagnetics Research*, vol. 105, pp. 15–30, 2010.
8. W.C. Chew, J. Jin, E. Michielssen, and J. Song, *Fast and Efficient Algorithms in Computational Electromagnetics*. Artech House, 2001.
9. I. Bogaert, J. Peeters, and F. Olyslager, "A nondirective plane wave MLFMA stable at low frequencies," *IEEE Transactions on Antennas and Propagation*, vol. 56, no. 12, pp. 3752–3767, December 2008.
10. J. Peeters, K. Cools, I. Bogaert, F. Olyslager, and D. De Zutter, "Embedding Calderón multiplicative preconditioners in multilevel fast multipole algorithms," *IEEE Transactions on Antennas and Propagation*, vol. 58, no. 4, pp. 1236–1250, April 2010.

11. I. Bogaert and F. Olyslager, "A low frequency stable plane wave addition theorem," *Journal of Computational Physics*, vol. 228, no. 4, pp. 1000–1016, March 2009.
12. ——, "New plane wave addition theorems," in *Proceedings of the 3rd International Conference on Mathematical Modeling of Wave Phenomena*, Växjö, Sweden, June 2008.
13. ——, "New plane wave addition theorems," in *AIP Conference Proceeding 1106*, 3rd International Conference on Mathematical Modeling of Wave Phenomena, Växjö, Sweden, June 2008, pp. 46–55.
14. V. Rokhlin, "Sparse diagonal forms for translation operators for the Helmholtz equation in two dimensions," *Research report YALEU/DCS/RR-1095*, Dec 1995.
15. S. Ohnuki and W. Chew, "Numerical Accuracy of Multipole Expansion for 2-D MLFMA," *IEEE Transactions on Antennas and Propagation*, vol. 51, no. 8, pp. 184–188, August 2003.
16. M. Hastriter, S. Ohnuki, and W. Chew, "Error Control of the Translation Operator in 3D MLFMA," *Microwave and Optical Technology Letters*, vol. 37, no. 3, pp. 184–188, May 2003.
17. S. D. Rao, D. R. Wilton, and A. W. Glisson, "Electromagnetic scattering by surfaces of arbitrary shape," *IEEE Trans. Antennas Propag.*, vol. AP-30, no. 3, May 1982.
18. G.H. Golub and C.F. Van Loan, *Matrix Computations (3rd edition)*. Johns Hopkins University Press, 1996.